Modeling and iterative pulse-shape control of optical chirped pulse amplifiers

authored by **A. Deutschmann, P. Malevich, A. Baltuska, and A. Kugi**

and published in *Automatica*.

Modeling and Iterative Pulse-Shape Control of Optical Chirped Pulse Amplifiers

Andreas Deutschmann [a] Pavel Malevich [b] Andrius Baltuška [b] Andreas Kugi [a]

[a] *Automation and Control Institute, Complex Dynamical Systems Group, TU Wien, Vienna, Austria*

[b] *Photonics Institute, Ultrafast Laser Group, TU Wien, Vienna, Austria*

Abstract

In this paper, we present an iterative learning algorithm for pulse-shape control applications of optical chirped pulse amplifiers for ultra-short, high-energy light pulses. For this, we first introduce a general nonlinear and infinite-dimensional mathematical model of chirped pulse amplifiers. By reducing the complexity of this detailed model and reformulating the control task, we are subsequently able to apply inversion-based iterative learning control to track desired output pulses. Using the reduced model to estimate both internal states and unknown parameters yields a fast and simple way of consistently estimating the input-output behavior without relying on a calibrated system model. The effectiveness of the resulting adaptive algorithm is finally illustrated with simulation scenarios on an experimentally validated mathematical model.

Key words: Chirped pulse amplifier, pulse-shape control, iterative learning control, infinite-dimensional systems.

1 Introduction

Over the last several decades, the systematic generation, detection, and manipulation of light opened a novel and rapidly growing field of research, now commonly known as photonics. However, the contributions of control engineering to this field are comparatively scarce with some exceptions like the control of mode-locked lasers [3], pulse shaping [28,20,21] and pulse propagation [18]. One particular task in photonic applications is the amplification of light pulses, especially for ultra-short high-energy pulses as used in strong field physics [12], for coherent control [9] or for pumping of optical parametric amplifiers [15]. The amplification of high-energy pulses is usually done by multipass amplification [14] using regenerative amplifiers (RAs), where a (usually) continuously pumped gain medium is placed inside an optical resonator. The pulse is then cycled several times until the stored energy of the gain medium is extracted and the amplified pulse is released. Since the amplification of intense laser pulses in active gain media is limited in its maximum energy due to self-focusing effects, a common technique to amplify high-energy pulses is to use so-called optical chirped pulse amplifiers (CPAs) [24]. The idea of CPAs is to stretch the incident pulse to reduce its power density and amplify the stretched pulse. This stretching can be achieved by introducing large amounts of artificial positive dispersion and thus convert the incident pulse into a chirped pulse. Afterwards, one wishes to recompress the chirped pulse by applying negative dispersion [26]. While this is possible for RAs with spectrally uniform gain, the quality of the amplified pulse is degrading rapidly for non-uniform gain which is typically the case for broad-band amplifiers needed for ultra-short pulse amplification. To approximately compensate for non-uniform gain and resulting effects like gain-narrowing [11], spectral filters in front of the RA [15] or within the resonator [13] have been successfully applied to achieve spectrally broad and thus temporally short pulses after recompression. However, these filters have to be adapted individually for each point of operation. The availability of programmable spectral filters for pulse shaping [29,25] makes the compensation by automatic control strategies a desirable option.

In general, the applications of control theory to problems in photonics mostly utilize model-free concepts like extremum-seeking (ES) [3,21] or some kind of genetic

⋆ This paper was not presented at any IFAC meeting. Corresponding author A. Deutschmann Tel. +43 (1) 58801 - 376 263.

Email addresses: deutschmann@acin.tuwien.ac.at (Andreas Deutschmann), pavel.malevich@tuwien.ac.at (Pavel Malevich), andrius.baltuska@tuwien.ac.at (Andrius Baltuška), kugi@acin.tuwien.ac.at (Andreas Kugi).

Preprint submitted to Automatica *25 July 2018*

Post-print version of the article: A. Deutschmann, P. Malevich, A. Baltuska, and A. Kugi, "Modeling and iterative pulse-shape control of optical chirped pulse amplifiers", *Automatica*, vol. 98, pp. 150–158, 2018, ISSN: 0005-1098. DOI: 10.1016/j.automatica.2018.09.002

algorithm [18] or model-free versions of iterative learning control (ILC) [20]. This is typically reasoned by two arguments, namely the degree of uncertainty inherent to some parameter values and the highly complex effects of the nonlinear and infinite-dimensional dynamics involved. In [20], a PD-type ILC is used to find the input pulse necessary to obtain a desired output pulse for an (unchirped) single-pass amplifier with spectrally uniform gain. Unlike such amplifiers, the CPA systems considered in this paper exhibit a variety of effects that make them quite challenging from a control point of view, e.g., extremely high gain levels that are saturating in a spectrally inhomogeneous way and nonlinear dispersive effects of the pulse propagation. Additionally, CPAs are typically operated in a regime where subsequent pulses are coupled as the stored energy of the gain medium is not allowed to fully recover in between two pulses. This can even induce an unstable system behavior [10]. From a control perspective, CPAs constitute a challenging class of systems. Accordingly, the main contribution of this paper lies in the introduction of a novel and challenging application to the control audience, the derivation of a comprehensive mathematical model and the development and evaluation of tailored ILC concepts on an experimentally validated model.

In this paper, we present a pulse-shape control for optical CPAs to track desired output pulses by means of inversion-based ILC. For this, we start by deriving a detailed nonlinear mathematical model of the process describing the evolution of the light field in Section 2. Section 3 then deduces a simplified linear model upon which the inversion-based ILC strategy is developed. The effectiveness of the inversion-based ILC strategy is then verified by simulation scenarios in Section 4 and some final conclusions are drawn in Section 5.

1.1 Mathematical Framework and Nomenclature

Before beginning to derive a complete mathematical model of the CPA, some preliminary statements will be made. In ultra-fast optics it is common to represent field quantities as real parts of complex quantities $\mathcal{A}$ that are described by complex envelope representations. For a plane wave with fixed polarization propagating along the z axis, this can be written as $\mathcal{A}(z,t) = A(z,t)\,\mathrm{e}^{-i(k_0 z - \omega_0 t)}$, with the complex pulse envelope $A(z,t)$ of a carrier wave, the time t, the spatial coordinate z, the imaginary unit i, the angular frequency ω_0 and the spatial wave number k_0. Since the pulses of interest are typically signals where the spatial and temporal variations of the complex pulse envelope are slow compared to the carrier oscillations, the approximations $\left|\frac{\partial^2 A(z,t)}{\partial z^2}\right| \ll \left|k_0 \frac{\partial A(z,t)}{\partial z}\right|$ and $\left|\frac{\partial^2 A(z,t)}{\partial t^2}\right| \ll \left|\omega_0 \frac{\partial A(z,t)}{\partial t}\right| \ll \left|\omega_0^2 A(z,t)\right|$ usually called slowly varying envelope approximation (SVEA), see, e.g., [23, Sec. 24.4] or [19], are applied. To analyze a pulse

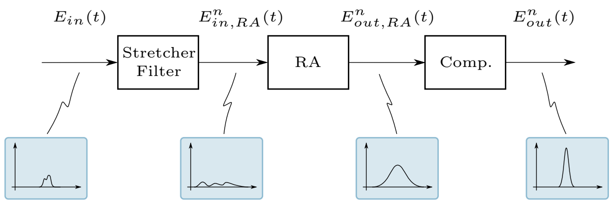

Fig. 1. Components of a CPA system and associated pulses. The schematic graphs in blue illustrate the ideal temporal pulse shapes for a desired Gaussian output pulse.

spectrally, the Fourier transform $\hat{\mathcal{A}}(z,\omega) = \mathfrak{F}\{\mathcal{A}(z,t)\}$ is used. All considered pulses at some location z_0 are bounded and of finite energy and thus $\mathcal{A}(z_0,\cdot) \in L^2 \cap L^\infty$ with the common norms

$$\|\mathcal{A}(z_0,\cdot)\|_2^2 = \|A(z_0,\cdot)\|_2^2 = \int_{-\infty}^{\infty} |A(z_0,t)|^2 \mathrm{d}t \tag{1a}$$

$$\|\mathcal{A}(z_0,\cdot)\|_\infty = \|A(z_0,\cdot)\|_\infty = \sup_{t\in\mathbb{R}} |A(z_0,t)| \,. \tag{1b}$$

Following the convention to describe the light pulse using the electric field $\mathcal{E}$, its pulse energy at z_0 is given by $W = {}^{A_B}/_{2Z_0}\|E(z_0,\cdot)\|_2^2 = {}^{A_B}/_{4\pi Z_0}\|\hat{E}(z_0,\cdot)\|_2^2$, where Z_0 denotes the impedance of free space and A_B is the cross section of the laser beam. In the sequel, spatial mean values over the length of the gain medium L are denoted by an overline, i.e. $\overline{N} = {}^1/_L \int_0^L N(z)\mathrm{d}z$.

2 Mathematical Model

Apart from the source of input pulses, a CPA system consists of three main components: a pulse stretcher with a spectral filter afterwards, a regenerative amplifier (RA) and a pulse compressor at the end. Such CPA systems are usually operated in a repetitive fashion, where identical seed pulses $E_{\mathrm{in}}(t)$ at a repetition frequency f_{rep} are fed into a (typically grating-based) pulse stretcher. Depending on the settings of the spectral filter and the state of the RA, this gives a heavily chirped pulse $E^n_{\mathrm{in,RA}}(t)$ which is amplified to $E^n_{\mathrm{out,RA}}(t)$ and compressed back to yield the output pulse $E^n_{\mathrm{out}}(t)$. The overall goal is to adjust the amplitude and phase characteristic of the spectral filter such that $E^n_{\mathrm{out,RA}}(t)$ is compressed back into an unchirped pulse of desired shape $E^{\mathrm{d}}_{\mathrm{out}}(t)$ as indicated in Fig. 1. While pulse stretchers and compressors can be easily described in terms of their spectral properties, the behavior of RAs is quite complex and requires a more detailed model. Thus, we start by addressing the description of the stretcher, the compressor and the spectral filter in Section 2.1 and then continue with the RA in Section 2.2.

2.1 Stretcher, Filter and Compressor

The basic idea of grating-based pulse stretchers (and compressors) is to vary the spatial paths depending on

Post-print version of the article: A. Deutschmann, P. Malevich, A. Baltuska, and A. Kugi, "Modeling and iterative pulse-shape control of optical chirped pulse amplifiers", *Automatica*, vol. 98, pp. 150–158, 2018, ISSN: 0005-1098. DOI: 10.1016/j.automatica.2018.09.002
The content of this post-print version is identical to the published paper but without the publisher's final layout or copy editing.

the frequency and thus introduce frequency-depending delays. When propagating through the device, each frequency component ω of the complex envelope's Fourier transform $\hat{E}(z,\omega)$ thus receives an additional phase $\varphi_{\mathrm{S}}(\omega)$ that can be approximated around the carrier frequency ω_0 with high accuracy by

$$\varphi_{\mathrm{S}}(\nu) = \varphi_{\mathrm{S},0} + \varphi_{\mathrm{S},1}\nu + \varphi_{\mathrm{S},2}\nu^2 + \varphi_{\mathrm{S},3}\nu^3 \qquad (2)$$

where $\nu = \omega - \omega_0$. The constants $\varphi_{\mathrm{S},i}$, $i \in \{0,1,2,3\}$ depend on the geometry, the pulse's center frequency ω_0 and the grating constant as shown in [26]. The transfer function of the pulse stretcher can therefore be written as $G_{\mathrm{S}}(\omega) = \eta_{\mathrm{S}}\, \mathrm{e}^{i\varphi_{\mathrm{S}}(\omega-\omega_0)}$ with the spectrally uniform efficiency coefficient η_{S}. Thus, the input pulse to the RA is given by

$$E^n_{\mathrm{in,RA}}(t) = \mathfrak{F}^{-1}\left\{G^n_{\mathrm{F}}(\omega)\, G_{\mathrm{S}}(\omega)\, \hat{E}_{\mathrm{in}}(\omega)\right\}, \qquad (3)$$

where $G^n_{\mathrm{F}}(\omega)$ denotes the adjustable transfer function of the spectral filter (set for the n-th pulse). Since the filter is not able to amplify any frequency component, its transfer function has to fulfill the constraint

$$|G^n_{\mathrm{F}}(\omega)| \leq 1 \qquad (4)$$

for all $\omega \in \mathbb{R}$. Analogously, the compressor can be described by $E^n_{\mathrm{out}}(t) = \mathfrak{F}^{-1}\left\{G_{\mathrm{C}}(\omega)\, \hat{E}^n_{\mathrm{out,RA}}(\omega)\right\}$ with $G_{\mathrm{C}}(\omega) = \eta_{\mathrm{C}}\, \mathrm{e}^{i\varphi_{\mathrm{C}}(\omega-\omega_0)}$ and φ_{C} according to (2).

Remark 1 *Analyzing the effect of* (2) *shows that the constant and linear terms introduce a phase shift and a time delay to the incident pulse, which can be neglected when studying the pulse shape, i.e.* $\varphi_{C,0} = \varphi_{S,0} = 0$ *and* $\varphi_{C,1} = \varphi_{S,1} = 0$*. The quadratic term produces the desired linear chirp while the cubic term generates a nonlinear chirp that typically becomes relevant for very short pulses below* 20 fs *[17].*

Depending on the source of seed pulses, a general incident pulse $E_{\mathrm{in}}(t)$ is showing some amount of chirp. Thus, the pulse stretcher only adds such an amount of quadratic phase that the desired temporal stretching is achieved. The compressor is then designed such that it compensates the overall quadratic and cubic phase components to achieve a "Fourier-limited" (unchirped) pulse. For simplicity it is assumed that the input pulse exhibits hardly any quadratic or cubic phase components and that stretcher and compressor compensate each other in a perfect way, i.e.

$$\varphi_{\mathrm{C},2} = -\varphi_{\mathrm{S},2}, \quad \varphi_{\mathrm{C},3} = -\varphi_{\mathrm{S},3}\,. \qquad (5)$$

2.2 Regenerative Amplifier

The central part of a CPA system is the RA, which comprises a (usually) continuously pumped gain medium located inside an optical resonator. Depending on the exact specifications, the optical resonator may be designed such that the pulse is injected into the gain medium bidirectionally or unidirectionally. In the following, we will restrict ourselves to unidirectional RAs since the bidirectional case can be treated similarly with slight modifications. According to Fig. 2, the n-th chirped pulse $E^n_{\mathrm{in,RA}}(t)$ leaving the pulse stretcher and filter is injected into the ring cavity and amplified by the gain medium. The k-th cycle of the n-th pulse is denoted by $E^{n,k}_{\mathrm{in,RA}}(t)$ prior to amplification and $E^{n,k}_{\mathrm{out,RA}}(t)$ after amplification. After N_{RC} cycles, the amplified pulse $E^n_{\mathrm{out,RA}}(t)$ is extracted and passed on to the pulse compressor. Until the next pulse arrives, the depleted population inversion is slowly regenerated (see Fig. 3 at the top). For simplification, losses of all optical components are combined in the efficiency coefficient η_{RC} acting on the recirculated pulse as shown in Fig. 2.

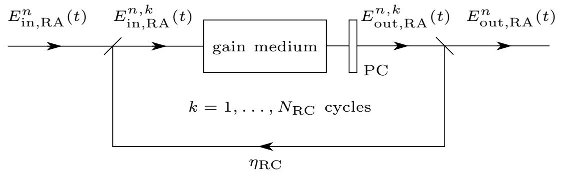

Fig. 2. Simplified layout of a unidirectional RA. The n-th chirped input pulse $E^n_{\mathrm{in,RA}}(t)$ is inserted into the ring cavity, amplified by passing the gain medium for N_{RC} times, and finally extracted by switching the polarization via a Pockels cell (PC). All losses are considered to be concentrated into the efficiency coefficient η_{RC}.

A mathematical model describing the amplification process needs to take into account the coupling of the doped ions inside the gain medium with the laser pulse and the continuous pumping light field. Additionally, the propagation of ultra-short and high-energy pulses in dense media is subject to nonlinear and dispersive effects that have to be taken into account. Due to the high energy and broad spectrum of the amplified pulses, the field-matter interaction while traveling through the gain medium is quite complex and results in fast dynamics of the excited ions. The effect of the several orders of magnitude weaker pumping field is negligible for the comparatively short period it takes the pulse to propagate through the gain medium. In contrast, during the regeneration time or in between cycles where no pulse is present in the gain medium, the pumping field's interaction with the ions is essential although quite simple and rather slow. Thus, it is advisable to split both domains and use separate pulse and pump models. Since the temporal pulse length is significantly smaller than its round-trip time within the cavity this is easily possible in a temporally consecutive fashion as shown in Fig. 3. To keep the following presentation short and compact, we will not explicitly specify space or time dependence of any variables unless it is required for the understanding.

Post-print version of the article: A. Deutschmann, P. Malevich, A. Baltuska, and A. Kugi, "Modeling and iterative pulse-shape control of optical chirped pulse amplifiers", *Automatica*, vol. 98, pp. 150–158, 2018, ISSN: 0005-1098. DOI: 10.1016/j.automatica.2018.09.002
The content of this post-print version is identical to the published paper but without the publisher's final layout or copy editing.

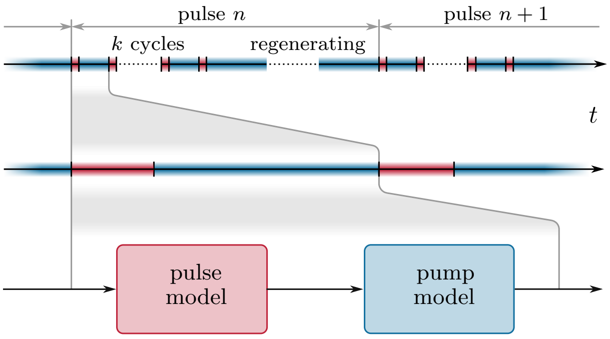

Fig. 3. Time sequence of a pulse amplification process. Red indicates times where the pulse is traveling through the gain medium while during blue time intervals the gain medium is exposed to the pumping laser only. The whole amplification process can thus be described by an alternating chain of pulse and pump models.

2.2.1 Pulse propagation in gain media (pulse model)

The propagation of light within media is determined by Maxwell's equations. To obtain a simplified description for pulses propagating along the z-direction in the presence of dispersive and nonlinear effects, the standard approach is to use the complex envelope representation and approximate the dispersion relation with a second order Taylor expansion (see, e.g., [22, pp. 991] or [19, Sec. 3.2]). By using a retarded time frame traveling with the pulse center at the group velocity v_{g}, one obtains the polarization driven version of the nonlinear Schrödinger equation (NLSE) (see [1,27])

$$i\frac{\partial E}{\partial z} + \frac{k_2}{2}\frac{\partial^2 E}{\partial t^2} - \frac{1}{2}\omega_0\varepsilon_0 n_0 n_2 |E|^2 E = \frac{\omega_0^2}{2c_0^2\varepsilon_0 k_0}P_{\mathrm{at}}, \quad (6)$$

with the refractive indices n_0, n_2, the dispersion coefficient k_2, the polarization induced by the dopant P_{at}, the permittivity of free space ε_0, and the vacuum speed of light c_0.

While equation (6) is describing the propagation of the electric field, a model for the atomic polarization of the dopant P_{at} is missing. This could be achieved by invoking the density operator formalism and the resulting von-Neumann equation. In this paper, we apply the intuitive and standard approach for laser systems to describe the system dynamics in terms of population densities and polarizations [23]. Without loss of generality, a Holmium-doped yttrium aluminum garnet (Ho:YAG) gain medium - a promising candidate for mid-infrared laser systems [15] - is chosen for the following demonstration purposes. Taking existing measurement results on the structure of Ho:YAG's ground and first excited state manifold [2, Fig. 1], a simplified energy level diagram can be established as shown in Fig. 4. Thus, the simplified model assumes that there is one ground state E_0 and one upper state E_5 with four intermediate states

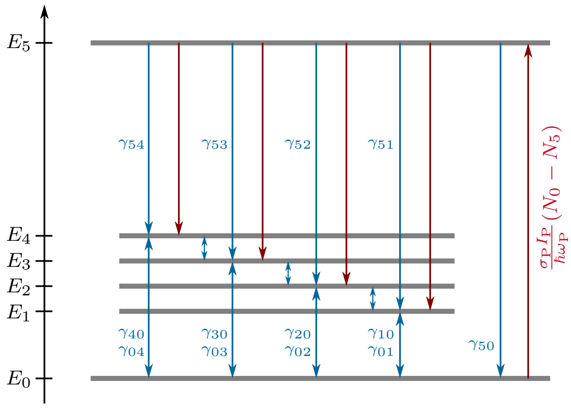

Fig. 4. Simplified energy level diagram for Ho:YAG with five resonant transitions in red and eleven radiative and non-radiative relaxation transitions in blue (see [2, Fig. 1]). For relaxation transitions, double arrows indicate downward and upward relaxation.

E_1 to E_4 where each level is populated by the associated population density N_0 to N_5. Each of the intermediate states is connected to the upper state by a resonant transition that lies within the frequency spectrum of our laser pulse while the resonant transition between the ground and the upper state is used for pumping. Thus, assuming homogeneously broadened line shapes, the polarization at every point z due to the resonant transition $j \leftrightarrow 5, j \in \{1, \dots, 4\}$ with the population densities N_j and N_5 is given by the resonant dipole equation [23]

$$\frac{\partial^2 \mathcal{P}_j}{\partial t^2} + \Delta\omega_j \frac{\partial \mathcal{P}_j}{\partial t} + \omega_j^2 \mathcal{P}_j = \kappa_j (N_j - N_5)\mathcal{E}, \quad (7)$$

with the transition's resonant frequency ω_j, its spectral width $\Delta\omega_j$, $\kappa_j = \frac{\omega_j \varepsilon_0 c_0 \Delta\omega_j \sigma_j}{\omega_0}$, and the transition cross section σ_j. Applying the envelope representation to (7) and using the SVEA yields

$$\frac{\partial P_j}{\partial t} = -\frac{\omega_j^2 + i\omega_0\Delta\omega_j - \omega_0^2}{\Delta\omega_j + i2\omega_0}P_j + \frac{\kappa_j}{\Delta\omega_j + i2\omega_0}(N_j - N_5)E\,. \quad (8)$$

The atomic polarization is then the sum of all four contributions, i.e. $P_{\mathrm{at}} = P_1 + P_2 + P_3 + P_4$. The time in which the pulse is traveling through the gain medium is significantly smaller than any dynamics of the pumping or non-radiative relaxation processes. Therefore, both can be neglected when describing the evolution of the population densities. Since the total number of the population is given by the dopant density, i.e.

$$\sum N_j = N_0 + N_1 + \ldots + N_5 = N_{\mathrm{tot}}, \quad (9)$$

it is sufficient to describe the densities of five energy levels. Thus, an energy conservation argument (see [23,

Post-print version of the article: A. Deutschmann, P. Malevich, A. Baltuska, and A. Kugi, "Modeling and iterative pulse-shape control of optical chirped pulse amplifiers", *Automatica*, vol. 98, pp. 150–158, 2018, ISSN: 0005-1098. DOI: 10.1016/j.automatica.2018.09.002
The content of this post-print version is identical to the published paper but without the publisher's final layout or copy editing.

Cha. 24]) gives the atomic rate equations

$$\frac{\partial N_j}{\partial t} = +\frac{1}{2\hbar}\mathrm{Im}\left\{E^* P_j\right\}, \quad j = 1, \dots, 4 \tag{10a}$$

$$\frac{\partial N_5}{\partial t} = -\frac{1}{2\hbar}\mathrm{Im}\left\{E^*(P_1 + P_2 + P_3 + P_4)\right\}, \tag{10b}$$

with the reduced Planck constant $\hbar$ and the complex conjugate electric field intensity E^*.

Summing up the results, the propagation of the k-th round trip in the ring cavity of the n-th pulse can be described by (6), (8) and (10) together with the initial and boundary conditions

$$\begin{aligned} E(0,t) &= E^{n,k}_{\mathrm{in,RA}}(t), & P_j(z,0) &= 0, \\ E(z,0) &= \frac{\partial E}{\partial t}(z,0) = 0, & N_j(z,0) &= N^{n,k}_{j,\mathrm{pulse}}(z), \end{aligned} \tag{11}$$

where $N^{n,k}_{j,\mathrm{pulse}}(z)$ denotes the population density of the j-th energy level at the location z at the time when the n-th pulse enters the gain medium for the k-th cycle. The amplified pulse is given by

$$E^{n,k}_{\mathrm{out,RA}}(t) = E(L,t) \tag{12}$$

where L is the length of the gain medium. The depleted population density after the pulse has passed is formally given by $N^{n,k}_{j,\mathrm{dep}}(z) = \lim_{t\to\infty} N^{n,k}_j(z,t)$. Since the total pulse width is finite in all practical applications, the remaining population density is also attained in finite time. The well-posedness and regularity of the boundary value problem of the NLSE alone has been recently studied in [5]. For more details on the well-posedness of general Maxwell-Bloch equations, we refer the interested reader to [16].

2.2.2 *Interaction with pumping field (pump model)*

During times where the light pulse is not present in the gain medium, the dynamics of the regeneration process is determined by the pumping laser and the redistribution of population densities due to non-radiative and radiative relaxation processes. Using the directed relaxation probability γ_{ij} from i to j and describing the pumping field only in terms of its field intensity I_{P} yields the atomic rate equations

$$\begin{aligned}
\frac{\partial N_1}{\partial t} &= -(\gamma_{10}+\gamma_{12})N_1+\gamma_{21}N_2+\gamma_{51}N_5+\gamma_{01}N_0 \\
\frac{\partial N_2}{\partial t} &= \gamma_{12}N_1-(\gamma_{20}+\gamma_{21}+\gamma_{23})N_2+\gamma_{32}N_3+\gamma_{52}N_5+\gamma_{02}N_0 \\
\frac{\partial N_3}{\partial t} &= \gamma_{23}N_2-(\gamma_{30}+\gamma_{32}+\gamma_{34})N_3+\gamma_{43}N_4+\gamma_{53}N_5+\gamma_{03}N_0 \\
\frac{\partial N_4}{\partial t} &= \gamma_{34}N_3-(\gamma_{40}+\gamma_{43})N_4+\gamma_{54}N_5+\gamma_{04}N_0 \\
\frac{\partial N_5}{\partial t} &= -(\gamma_{50}+\gamma_{51}+\gamma_{52}+\gamma_{53}+\gamma_{54})N_5+\frac{\sigma_{\mathrm{P}} I_{\mathrm{P}}}{\hbar\omega_{\mathrm{P}}}(N_0-N_5),
\end{aligned} \tag{13}$$

with the pumping field's cross section σ_{P} and its angular frequency ω_{P}. The population of the ground state N_0 can be eliminated by (9). Using the Frantz-Nodvik approach [6][23, Cha. 10] for a continuous pumping process and assuming a steady-state solution of the field intensity results in

$$\frac{\partial I_{\mathrm{P}}}{\partial z} = \sigma_{\mathrm{P}}(N_5 - N_0)I_{\mathrm{P}}, \tag{14}$$

with the initial and boundary conditions $I_{\mathrm{P}}(0,t) = I_0$ and $N_j(z,0) = N^{n,k}_{j,\mathrm{pump}}(z)$ where $N^{n,k}_{j,\mathrm{pump}}(z)$ denotes the population of the j-th level at the beginning of the k-th cycle of the n-th pulse. The final regenerated population density is given at the time it takes the pulse to complete the round trip, i.e. $N^{n,k}_{j,\mathrm{reg}}(z) = N_j(t_{\mathrm{end}}, z)$ whereby $t_{\mathrm{end}} = {}^{(L_{\mathrm{RC}}-L)}/_{c_0}$, with the length of the ring cavity L_{RC}.

2.2.3 *Coupling of pulse and pump model*

From a functional point of view, the pulse model is taking the input pulse $E^{n,k}_{\mathrm{in,RA}}(t)$ and the corresponding initial population distribution $N^{n,k}_{j,\mathrm{pulse}}(z)$ and computes an amplified pulse $E^{n,k}_{\mathrm{out,RA}}(t)$ (that is assumed to be bounded and of finite energy again) and a remaining population distribution $N^{n,k}_{j,\mathrm{dep}}(z)$. The pump model on the other hand is taking this remaining population distribution (and the given incident pumping intensity I_0) and integrates the rate equation (13) to obtain $N^{n,k}_{j,\mathrm{reg}}$.Taking into account the concentrated losses of the cavity according to Fig. 2, the coupling conditions are given by

$$N^{n,k}_{j,\mathrm{pump}}(z) = N^{n,k}_{j,\mathrm{dep}}(z) \tag{15a}$$

$$E^{n,k+1}_{\mathrm{in,RA}}(t) = \eta_{\mathrm{RC}} E^{n,k}_{\mathrm{out,RA}}(t) \tag{15b}$$

$$N^{n,k+1}_{j,\mathrm{pulse}}(z) = N^{n,k}_{j,\mathrm{reg}}(z). \tag{15c}$$

Thus, the propagation of the n-th laser pulse can be described by an alternating application of pulse and pump model with the coupling conditions above until the output pulse is finally given by

$$E^{n}_{\mathrm{out,RC}}(t) = E^{n,N_{\mathrm{RC}}}_{\mathrm{out,RC}}(t) \tag{16}$$

and the remaining populations by $N^{n}_{j,\mathrm{out}}(z) = N^{n,N_{\mathrm{RC}}}_{j,\mathrm{dep}}(z)$. During the following main regeneration phase until the $(n+1)$-st pulse arrives, one can simply integrate the pump model for the remaining time

$$t_{\mathrm{reg}} = {}^{1}/_{f_{\mathrm{rep}}} - {}^{1}/_{c_0} N_{\mathrm{RC}} \left[L_{\mathrm{RC}} + {}^{(c_0 - v_{\mathrm{g}})}/_{v_{\mathrm{g}}} L\right] \tag{17}$$

given by the repetition frequency f_{rep}, the number of round trips N_{RC}, the physical dimensions L and L_{RC}, and the group velocity v_{g} to obtain the initial population densities for the following pulse, i.e. $N^{n+1,1}_{j,\mathrm{pulse}}(z)$.

Post-print version of the article: A. Deutschmann, P. Malevich, A. Baltuska, and A. Kugi, "Modeling and iterative pulse-shape control of optical chirped pulse amplifiers", *Automatica*, vol. 98, pp. 150–158, 2018, ISSN: 0005-1098. DOI: 10.1016/j.automatica.2018.09.002
The content of this post-print version is identical to the published paper but without the publisher's final layout or copy editing.

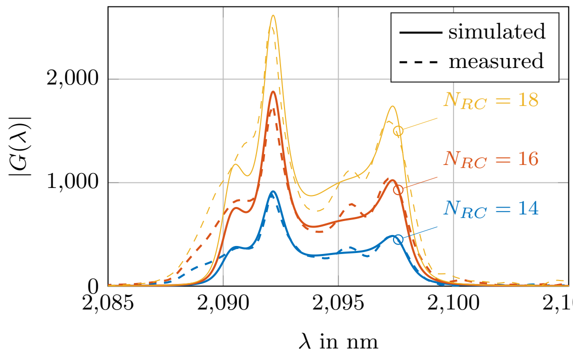

Fig. 5. Comparison of the amplifier gain $|G(\lambda)|$ as a function of the wavelength $\lambda = {}^{2\pi c_0}/_{\omega}$ between measurements and the simulated model for $N_{\mathrm{RC}} = 14$ (blue), $N_{\mathrm{RC}} = 16$ (red) and $N_{\mathrm{RC}} = 18$ (yellow).

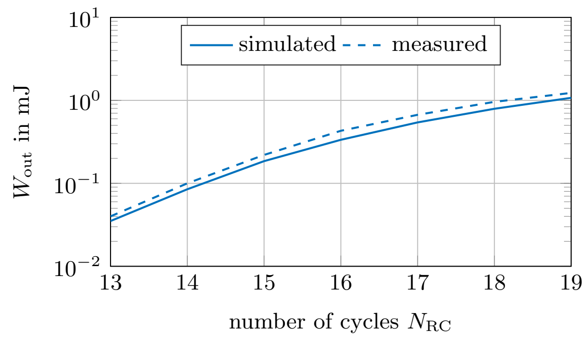

Fig. 6. Evolution of the steady-state output pulse energy W_{out} of the CPA system and the simulated model.

2.2.4 Validity and properties of the CPA model

In order to establish the validity of the proposed CPA model, we want to compare it to actual measurement data from a Ho:YAG system given in [15]. Without going into the details of the parameter identification, extracting suitable parameters - especially for the relaxation probabilities γ_{ij} - can be quite challenging. As shown in Fig. 5, the amplifier gain of the CPA system is adequately reproduced by the proposed mathematical model. Some resonant transitions other than the four considered seem to play only a minor role. In particular the gain for higher frequencies with wavelengths lower then 2090 nm suggests that some levels above the upper state E_5 are populated (see [2]) and contribute slightly to the overall gain. The effects of this additional gain can be seen in Fig. 6: while the saturation behavior itself in terms of the output energy of $E_{\mathrm{out}}(t)$ is nicely reproduced, a constant (multiplicative) error remains for various numbers of cycles N_{RC} in the ring cavity.

The proposed mathematical model for CPAs combines a number of interesting and challenging properties: First of all, the pulse propagation is governed by the antagonistic effects of dispersion and self-steepening due to the NLSE (6). CPA systems naturally exhibit a high-gain behavior with a strongly inhomogeneous gain characteristic (see Fig. 5) that is saturating due to the finite energy stored in the upper energy state. Since the gain characteristic involves several atomic transitions, this saturation effect is acting in a spectrally inhomogeneous fashion. The regeneration period is typically not sufficient to fully recover the depleted population inversion. As a result, the gain of the current pulse depends on the amount of energy extracted by the previous pulses. While this is the root cause for the saturation behavior in Fig. 6, the resulting inter-pulse coupling can be quite significant and - depending on the chosen parameter values - lead to an unstable or even chaotic behavior [4,10] of the CPA.

3 Control Strategy

Before starting with the control design itself, we restate the control objective, which is to adapt the adjustable input filter $G_{\mathrm{F}}^n(\omega)$ such that a desired output pulse $E_{\mathrm{out}}^d(t)$ is achieved. Since the filter is subject to the constraints (4), one is only able to generate pulses that can be sustained by the CPA system.

Due to the linearity of both stretcher and filter, one can separate the spectral filter and place it in front of the remaining system with the virtual input pulse $E_{\mathrm{v,in}}^n(t)$. Assuming that the input pulse $E_{\mathrm{in}}(t)$ is spectrally broad enough, a suitable transfer function of the filter can be easily written as

$$G_{\mathrm{F}}^n(\omega) = \frac{\hat{E}_{\mathrm{v,in}}^n(\omega)}{\hat{E}_{\mathrm{in}}(\omega)}. \tag{18}$$

The constraint of the spectral filter (4) thus results in an admissible set of virtual input pulses given by

$$|\hat{E}_{\mathrm{v,in}}^n(\omega)| \leq |\hat{E}_{\mathrm{in}}(\omega)| \tag{19}$$

for all $\omega \in \mathbb{R}$. This reformulates the control task as a problem of iteratively adjusting $E_{\mathrm{v,in}}^n(t)$ due to output measurements.

Using ILC to determine suitable pulses $E_{\mathrm{v,in}}^n(t)$ seems natural in this reformulated setting. In [20], a PD-type ILC law was used to apply pulse-shape control for a single-pass laser amplifier described by a simple Frantz-Nodvik model with uniform gain. Additionally, the initial population inversion is completely restored for each pulse, i.e different pulses are not coupled and the system behaves identical for each iteration. Even in this simplified scenario, PD-type ILC laws show a rather slow convergence. Considering the extremely high and variable amounts of gain exhibited by the more general CPA system considered in this article, one would expect painfully slow rates of convergence at best. In extensive simulation scenarios we could not manage to find a convergent PD-type law, which is mainly due to the dispersive effects of

Post-print version of the article: A. Deutschmann, P. Malevich, A. Baltuska, and A. Kugi, “Modeling and iterative pulse-shape control of optical chirped pulse amplifiers”, *Automatica*, vol. 98, pp. 150–158, 2018, ISSN: 0005-1098. DOI: 10.1016/j.automatica.2018.09.002
The content of this post-print version is identical to the published paper but without the publisher’s final layout or copy editing.

the NLSE. An inversion-based scheme seems more suitable for this particular task, but the complex nonlinear and infinite-dimensional behavior of the system limits the usability (as well as availability) of exact inversion methods. However, the main nonlinearity affecting the input-output behavior is introduced by the depletion of the population distributions (due to (8) and (10)). Such saturation effects are typically handled quite well by ILC schemes, wherefore an approximate inversion-based approach by using a reduced, linear model seems tractable.

Remark 2 *By applying ILC methods, we are tacitly neglecting the coupling of subsequent pulses and limit our focus solely on the pulse-shaping task while treating the coupling as a minor variation of the system behavior. This is fine for weakly coupled pulses where the CPA is operated in a stable regime. In general, however, this analysis falls short of capturing the full picture and a more elaborated approach is deemed necessary.*

3.1 Reduced linear input-output behavior

The main idea to obtain a simplified input-output behavior is to neglect the complex population dynamics and calculate the pulse evolution by an approximate linear model. Equivalently, one can linearize the pulse evolution model (6) and (8) around $E(z,t) = P_j(z,t) = 0$ and a stationary solution $N_j^0(z)$ of the pump model (13) and (14). Henceforth, we make the following assumptions:

Assumption 1 *The influence of the nonlinear polarization due to the Kerr effect (i.e., the term proportional to $|E|^2E$ in (6)) can be neglected.*

This assumption is typically fulfilled since CPA systems use the stretcher/compressor arrangement to avoid the intensity regime where strong Kerr effects take place.

Assumption 2 *The population densities remain at the stationary, unsaturated level $N_j^0(z)$ for all N_{RC} cycles and all pulses.*

As long as the overall pulse energy inside the cavity remains comparatively low (below 100 µJ for the given system), the amplifier is not saturating and the steady-state population remains close to its stationary level, i.e. $N_j^{\mathrm{ss}}(z) \approx N_j^0(z)$. This is clearly not the case for operation scenarios with high energy pulses close to the capabilities of the CPA system. As a consequence, Assumption 2 will be relaxed in Section 3.3 using an adaptive design.

Remark 3 *Note the difference between stationary (unsaturated) populations as stationary solutions to (14), i.e. when there is no depletion due to amplified pulses, and steady-state populations, i.e. the depleted population density for a fixed input pulse $E_{v,in}$ where the population loss due to the amplification process is exactly compensated by the regeneration process.*

Utilizing both assumptions, one ends up with a simplified linear pulse model

$$i\frac{\partial E}{\partial z} = -\frac{k_2}{2}\frac{\partial^2 E}{\partial t^2} + \frac{\omega_0^2}{2c_0^2\varepsilon_0 k_0}(P_1+P_2+P_3+P_4) \tag{20a}$$

$$\frac{\partial P_j}{\partial t} = -\frac{\omega_j^2 + i\omega_0\Delta\omega_j - \omega_0^2}{\Delta\omega_j + i2\omega_0}P_j - \frac{\kappa_j}{\Delta\omega_j + i2\omega_0}\Delta N_{5j}^0 E, \tag{20b}$$

where $\Delta N_{5j}^0 = N_5^0 - N_j^0$ is given by the stationary solution of (13), (14) and (9), which can be written in vector notation as

$$\mathbf{0} = \mathbf{\Gamma}_1(I_{\mathrm{P}}(z))\mathbf{N}^0(z) + \mathbf{\Gamma}_2(I_{\mathrm{P}}(z))N_{\mathrm{tot}} \tag{21a}$$

$$\frac{\partial I_{\mathrm{P}}(z)}{\partial z} = \sigma_{\mathrm{P}}\left(\begin{bmatrix}1 & 1 & 1 & 1 & 2\end{bmatrix}\mathbf{N}^0(z) - N_{\mathrm{tot}}\right)I_{\mathrm{P}}(z), \tag{21b}$$

where $\mathbf{N}^0(z) = [N_1^0(z), \ldots, N_5^0(z)]^{\mathrm{T}}$. Applying the Fourier-transform to (20b) yields the spectral description of the susceptibility of the j-th transition

$$\begin{aligned}\hat{P}_j(z,\omega) &= \frac{-\kappa_j(N_5^0(z) - N_j^0(z))}{i\omega(\Delta\omega_j + 2i\omega_0) + \omega_j^2 + i\omega_0\Delta\omega_j - \omega_0^2}\hat{E}(z,\omega) \\ &= \chi_j(\omega; \Delta N_{5j}^0(z))\,\hat{E}(z,\omega).\end{aligned} \tag{22}$$

With (22), the remaining equation (20a) can be solved analytically using (11) and (12) which gives the transfer function of a single pass $\hat{E}_{\mathrm{out,RA}}^{n,k}(\omega) = G_{\mathrm{sp}}(\omega; \overline{\Delta\mathbf{N}^0})\hat{E}_{\mathrm{in,RA}}^{n,k}(\omega)$ where

$$\begin{aligned}G_{\mathrm{sp}}\left(\omega; \overline{\Delta\mathbf{N}^0}\right) &= \exp\left[-i\int_0^L \frac{k_2}{2}\omega^2 \mathrm{d}z\right] \\ &\times\exp\left[-i\int_0^L \frac{\omega_0^2}{2c_0^2\varepsilon_0 k_0}\sum\nolimits_{j=1}^4 \chi_j\left(\omega; \Delta N_{5j}^0(z)\right)\mathrm{d}z\right] \\ &= \exp\left[-iL\left(\frac{k_2}{2}\omega^2 + \frac{\omega_0^2}{2c_0^2\varepsilon_0 k_0}\sum\nolimits_{j=1}^4 \chi_j\left(\omega; \overline{\Delta N_{5j}^0}\right)\right)\right],\end{aligned} \tag{23}$$

with $\overline{\Delta\mathbf{N}^0} = \left[\overline{\Delta N_{51}^0}, \ldots, \overline{\Delta N_{54}^0}\right]^{\mathrm{T}}$. Using (3), (15), (16), and (18) finally yields the overall transfer function of the reduced linear model

$$\begin{aligned}\hat{E}_{\mathrm{out}}^n(\omega) &= \eta_{\mathrm{S}}\eta_{\mathrm{C}}\eta_{\mathrm{RC}}^{N_{\mathrm{RC}}-1}G_{\mathrm{sp}}\left(\omega; \overline{\Delta\mathbf{N}^0}\right)^{N_{\mathrm{RC}}}\hat{E}_{\mathrm{v,in}}^n(\omega) \\ &= G\left(\omega; \overline{\Delta\mathbf{N}^0}\right)\hat{E}_{\mathrm{v,in}}^n(\omega),\end{aligned} \tag{24}$$

where the mean population inversion $\overline{\Delta\mathbf{N}^0}$ is a finite-dimensional parameter vector defining the overall gain of the CPA system - a fact that will be used later on.

Post-print version of the article: A. Deutschmann, P. Malevich, A. Baltuska, and A. Kugi, "Modeling and iterative pulse-shape control of optical chirped pulse amplifiers", *Automatica*, vol. 98, pp. 150–158, 2018, ISSN: 0005-1098. DOI: 10.1016/j.automatica.2018.09.002

3.2 Inversion-based ILC

We now want to track a desired output pulse $E^{\mathrm{d}}_{\mathrm{out}}(t) \in L^2(-\infty,\infty) \cap L^\infty(-\infty,\infty)$ by means of the virtual input $E^n_{\mathrm{v,in}}(t)$, using the reduced input-output behavior derived in the previous section, while being subject to the input constraints (19). The handling of input constraints can be done easily by projecting onto the set of feasible input signals (see, e.g., [8]). Thus, we consider a general learning law in the frequency domain

$$\hat{E}^{n+1}_{\mathrm{v,in}}(\omega) = \mathcal{T}\left[\hat{E}^n_{\mathrm{v,in}}(\omega) + L^n(\omega)\left(\hat{E}^{\mathrm{d}}_{\mathrm{out}}(\omega) - \hat{E}^n_{\mathrm{out}}(\omega)\right)\right] \tag{25}$$

with the n-th linear learning operator L^n and the nonlinear truncation operator $\mathcal{T}$ given by

$$\mathcal{T}\left(\hat{E}(\omega)\right) = \begin{cases}\hat{E}(\omega) & \text{if } |\hat{E}| \leq |\hat{E}_{\mathrm{in}}| \\ |\hat{E}_{\mathrm{in}}(\omega)| \exp\left(i \arg \hat{E}(\omega)\right) & \text{else.}\end{cases} \tag{26}$$

To obtain a suitable learning operator, a (regularized) inversion on an infinite time-horizon as shown in [7] could be applied. Using a frequency domain approach, the infinite-dimensional character of the reduced system does not cause any problems. However, due to the spectrally narrow high gain nature of the system, inversion-based learning laws yield particularly high learning gains in spectral regions where no signal is present and learning should be avoided. In view of unmodeled dynamics and in particular the neglected influence of the Kerr effect due to Assumption 1, it is inevitable to limit learning to those spectral regions where the input signal is expected to be strong. Adding additional spectral shaping to an inversion-based approach, the simple iteration-invariant learning operator is given as

$$L^n(\omega) = L(\omega) = \frac{1}{G(\omega; \overline{\Delta\mathbf{N}^0})} \frac{|\hat{E}^{\mathrm{d}}_{\mathrm{out}}(\omega)|^2}{N + |\hat{E}^{\mathrm{d}}_{\mathrm{out}}(\omega)|^2}, \tag{27}$$

with the shaping parameter $N \geq 0$ that separates spectral ranges where learning is desirable from those where learning should be avoided relative to $|\hat{E}^{\mathrm{d}}_{\mathrm{out}}(\omega)|^2$. Since programmable spectral filters are usually specified in the frequency domain, the ILC law can be implemented directly as given in (25) together with (18).

3.3 Adaptive inversion-based ILC

The inversion-based learning operator presented above suffers from two distinct problems: First, it uses the stationary mean population inversion $\overline{\Delta\mathbf{N}^0}$ due to Assumption 2 and therefore considerably overestimates the gain exhibited by the CPA system for high energy pulses. While this reduces the speed of convergence significantly, it can also impair the stability of the learning law, although simulation studies suggest that this is only the case for heavily saturating scenarios. Second, it requires an accurate and validated model of the CPA system, in particular of the gain medium, in order to obtain a good learning gain. However, as part of the ILC strategy we do know corresponding input and output measurements which can be used to adaptively estimate the CPAs current state. Thus, we relax Assumption 2 by replacing it with

Assumption 3 *The drop of the population densities during a single pass of the laser pulse can be neglected for the pulse propagation.*

Using this assumption, one is still able to describe the pulse evolution by the single pass gain function given in (23) with some initial mean population inversion denoted by $\overline{\Delta\mathbf{N}^1}$. For the following pass, the same relation will hold, but with some unknown depleted mean population inversion $\overline{\Delta\mathbf{N}^2}$. Proceeding this way, one ends up with a total gain similar to (24) given by $\tilde{G}\left(\omega; \overline{\Delta\mathbf{N}^1}, \dots, \overline{\Delta\mathbf{N}^{N_{\mathrm{RC}}}}\right) = \eta \prod_{k=1}^{N_{\mathrm{RC}}} G_{\mathrm{sp}}\left(\omega; \overline{\Delta\mathbf{N}^k}\right)$ with the unknown mean population inversions $\overline{\Delta\mathbf{N}^k}$ where $k = 1, \dots, N_{\mathrm{RC}}$ and $\eta = \eta_{\mathrm{S}}\eta_{\mathrm{C}}\eta_{\mathrm{RC}}^{N_{\mathrm{RC}}-1}$. Using the definition of χ_j in (22) one can rewrite the equation above as

$$\tilde{G}\left(\omega; \overline{\Delta\mathbf{N}^1}, \dots, \overline{\Delta\mathbf{N}^{N_{\mathrm{RC}}}}\right) = G\left(\omega; \overline{\Delta\mathbf{N}}\right) \tag{28}$$

where

$$\overline{\Delta\mathbf{N}} = \frac{1}{N_{\mathrm{RC}}} \sum_{k=1}^{N_{\mathrm{RC}}} \overline{\Delta\mathbf{N}^k} \tag{29}$$

denotes the averaged mean population inversions over the number of round trips N_{RC}. This shows that one can still use the reduced linear model derived in Section 3.1 when Assumption 2 is violated by replacing the stationary, unsaturated population inversions $\overline{\Delta\mathbf{N}^0}$ with averaged mean population inversions $\overline{\Delta\mathbf{N}}$ as long as Assumption 3 remains valid. This way, one effectively parametrizes the total transfer function of the reduced model by a finite set of parameters $\overline{\Delta\mathbf{N}} = \left[\overline{\Delta N_{51}}, \dots, \overline{\Delta N_{54}}\right]^{\mathrm{T}}$ equal to the number of resonant (lasing) transitions of the gain medium, i.e. in the case of Ho:YAG by four parameters. Thus, the CPA's transfer function for the n-th pulse can be estimated using the optimization problem

$$\Delta\mathbf{N}^n_{\mathrm{opt}} = \min_{\overline{\Delta\mathbf{N}}} J^n(\overline{\Delta\mathbf{N}}), \tag{30}$$

with the objective function $J^n(\overline{\Delta\mathbf{N}}) = \|\hat{E}^n_{\mathrm{out}}(\cdot) - G(\,\cdot\,; \overline{\Delta\mathbf{N}})\hat{E}^n_{\mathrm{v,in}}(\cdot)\|_2$ to find a suitable mean population inversion $\Delta\mathbf{N}^n_{\mathrm{opt}}$ such that $G(\omega; \Delta\mathbf{N}^n_{\mathrm{opt}})$ optimally reproduces the measured input-output behavior. The adaptive learning operator, see (27), is then given by

$$L^n(\omega) = \frac{1}{G(\omega; \Delta\mathbf{N}^n_{\mathrm{opt}})} \frac{|\hat{E}^{\mathrm{d}}_{\mathrm{out}}(\omega)|^2}{N + |\hat{E}^{\mathrm{d}}_{\mathrm{out}}(\omega)|^2}. \tag{31}$$

Post-print version of the article: A. Deutschmann, P. Malevich, A. Baltuska, and A. Kugi, "Modeling and iterative pulse-shape control of optical chirped pulse amplifiers", *Automatica*, vol. 98, pp. 150–158, 2018, ISSN: 0005-1098. DOI: 10.1016/j.automatica.2018.09.002

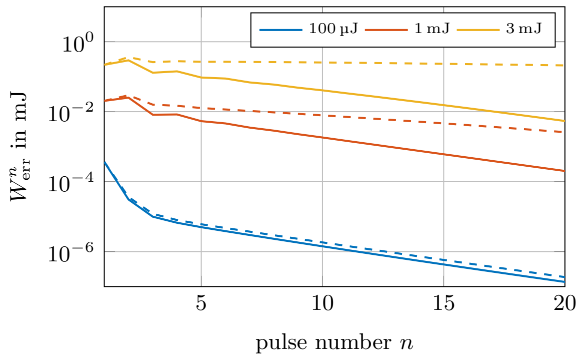

Fig. 7. Evolution of the error energy W_{err}^{n} for adaptive (solid line) and non-adaptive (dashed line) ILC strategies for a laser pulse with 100 µJ, 1 mJ and 3 mJ, respectively. For the 3 mJ pulse, the non-adaptive ILC strategy diverges eventually.

Since the pulse energy is equivalent to the squared L^2-norm, it is convenient to use the output error energy $W_{\mathrm{err}}^{n} = {}^{A_{\mathrm{B}}}/_{2Z_0} \left\| E_{\mathrm{out}}^{\mathrm{d}} - E_{\mathrm{out}}^{n} \right\|_2^2$ to illustrate the convergence behavior. In Fig. 7, the difference in convergence speed is shown for laser pulses with a total energy of 100 µJ, 1 mJ and 3 mJ, respectively. The initial population is chosen as a solution to (21), i.e. the CPA is fully pumped. The 100 µJ pulse is too weak to significantly deplete the population levels, wherefore the adaptive and the non-adaptive ILC strategy converge at roughly the same rate. The 1 mJ pulse produces some saturation effects but still both ILC strategies converge to the desired pulse, although with a significant difference in convergence speed. For the heavily saturating 3 mJ pulse, the non-adaptive ILC strategy accumulates phase errors due to the increasingly erroneous reduced model and eventually diverges. The adaptive ILC strategy on the other hand is producing the desired pulse perfectly.

The presented approach is a fast and simple way to consistently estimate the observed transfer function based on unknown population densities. Since the values of κ_j in (8) are rarely known, this approach is ultimately able to estimate the combined quantity $\kappa_j \Delta N_{5j}$. Moreover, it is easy to extend the optimization problem (30) such that it includes the unknown quantities ω_j and $\Delta\omega_j$ and possibly an overall scaling factor $\eta = \eta_{\mathrm{S}}\eta_{\mathrm{C}}\eta_{\mathrm{RC}}^{N_{\mathrm{RC}}-1}$. Thus, the proposed algorithm is able to handle arbitrary gain media without the burden of identifying the complex system dynamics. Only a given number of resonant lasing transitions is required which can be easily obtained from suitable measurements.

4 Simulation results for the experimentally validated model

To demonstrate the presented algorithm, we apply the adaptive ILC scheme (25), (26), (31) and (30) to the experimentally validated mathematical model derived in Section 2. As explained in Section 2.1, stretcher and compressor where chosen such that they compensate each other perfectly. As a result, the spectral filter $G_{\mathrm{F}}^{n}(\omega)$ has to compensate the quadratic phase due to the dispersion introduced by the NLSE (6). In practice, quadratic and cubic phase components are usually handled by adjusting the stretcher's phase coefficients $\varphi_{\mathrm{S},2}$ and $\varphi_{\mathrm{S},3}$ instead of using the spectral filter $G_{\mathrm{F}}^{n}(\omega)$. To visualize the fine details of the input filter's phase shift, we eliminated the quadratic and cubic phase components in the following plots for illustration purposes. The initial population densities before the first pulse enters the CPA system are assumed to be fully pumped and thus can be obtained by solving (21). Finally, the CPA system is seeded by (measured) 29.4 nJ pulses at a repetition rate of $f_{\mathrm{rep}} = 1\,\mathrm{kHz}$ and the pulse stays inside the resonator for $N_{\mathrm{RC}} = 23$ cycles.

The first simulation example shown in Fig. 8 considers a desired 3 mJ Gaussian pulse using a pumping source with 35 W (i.e., a pumping intensity I_0 of $6.96 \times 10^7\,\mathrm{W\,m^{-2}}$). As the population inversion is depleting due to the extracted energy, the input energy is increased until the input filter is limited by the constraints (4). As a result, the desired pulse shape cannot be exactly reached and the output error settles at a finite level. To exactly obtain the desired 3 mJ pulse, one would need to increase the pumping power. As mentioned above, the presented method is able to produce arbitrarily shaped pulses as long as the desired pulse is within the capabilities of both amplifier and input filter. Fig. 9 shows the learned input filter to obtain a superposition of three pulses with a total energy of 1.5 mJ.

5 Conclusions and Outlook

In this paper, we presented an adaptive strategy to produce desired pulses with optical chirped pulse amplifiers. The detailed nonlinear and infinite-dimensional model derived and validated in Section 2 was reduced such that its input-output behavior can be described by a transfer function that is characterized by the mean population densities of the gain medium. Introducing averaged mean population densities, one is able to consistently estimate the current state of the amplifier by solving an optimization problem. The benefit of this approach is that it can easily estimate not only the population densities but also all unknown parameters essential for the input-output behavior. This estimated transfer function can then be used to apply an inversion-based ILC scheme. Thus, one obtains an adaptive algorithm to track desired output pulses, which is structurally simple, fast and does not rely on parameters that are hard to identify. Apart from physical constants and quantities easily measurable, one only needs to specify the number of resonant transitions.

As CPAs exhibit a very complex and challenging system dynamics, the presented approach can only be con-

Post-print version of the article: A. Deutschmann, P. Malevich, A. Baltuska, and A. Kugi, "Modeling and iterative pulse-shape control of optical chirped pulse amplifiers", *Automatica*, vol. 98, pp. 150–158, 2018, ISSN: 0005-1098. DOI: 10.1016/j.automatica.2018.09.002
The content of this post-print version is identical to the published paper but without the publisher's final layout or copy editing.

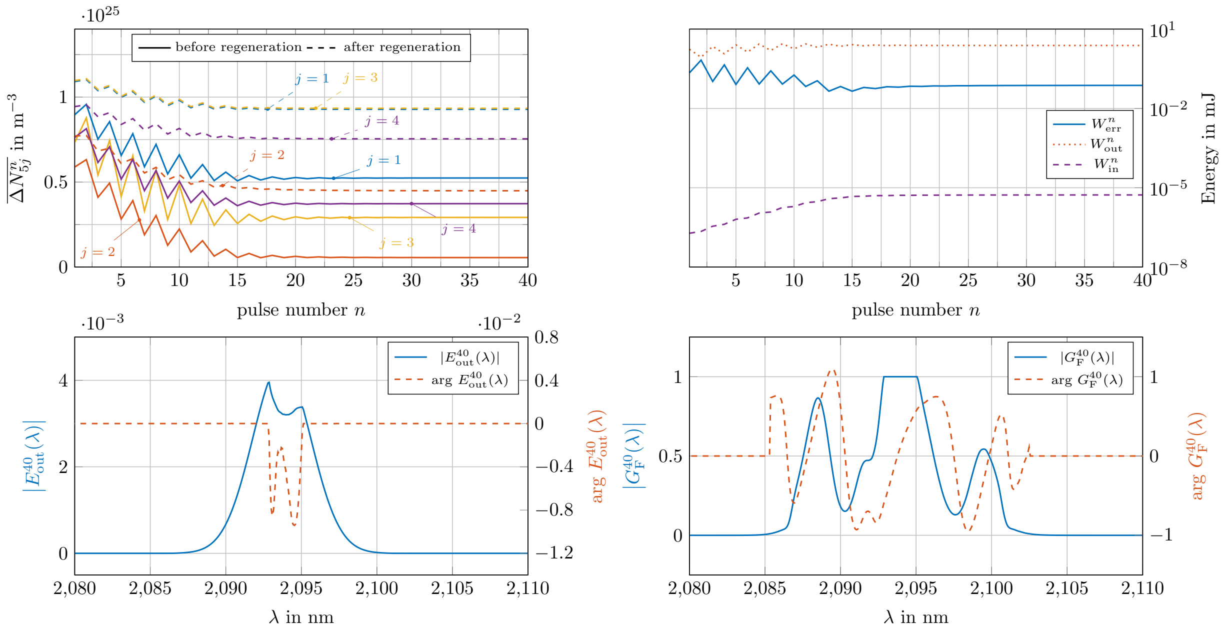

Fig. 8. Convergence behavior of a 3 mJ pulse at 35 W pumping power using $N = 10^{-9}$.

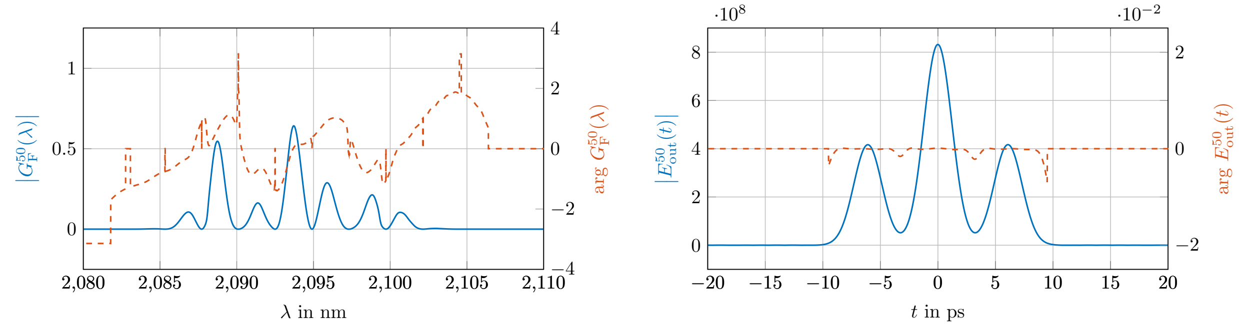

Fig. 9. Input filter $G^{50}_{\rm F}(\lambda)$ and the resulting output pulse $E^{50}_{\rm out}(t)$ for a desired superposition of three pulses using $N = 10^{-8}$.

sidered a first step and there are several open questions for future research. For example, the proposed approach is correcting the reduced model's errors due to neglecting the population depletion by using an adaptive ILC algorithm, existing model knowledge could be used to implement a type of observer-based scheme to predict effects of the population dynamics. Additionally, a rigorous stability analysis including the coupling of subsequent pulses is clearly desirable and could be used to include feedback stabilization of otherwise unstable operational regimes.

References

[1] G. P. Agrawal and N. A. Olsson. Self-phase modulation and spectral broadening of optical pulses in semiconductor laser amplifiers. *IEEE J Quant Electron*, 25(11):2297–2306, 1989.

[2] D. C. Brown, V. Envid, and J. Zembek. Ho:YAG absorption cross sections from 1700 to 2200 nm at 83, 175, and 295 K. *Appl Optic*, 51(34):8147–8158, 2012.

[3] S. L. Brunton, X. Fu, and J. N. Kutz. Extremum-Seeking Control of a Mode-Locked Laser. *IEEE J Quant Electron*, 49(10):852–861, 2013.

[4] J. Dörring, A. Killi, U. Morgner, A. Lang, M. Lederer, and D. Kopf. Period doubling and deterministic chaos in continuously pumped regenerative amplifiers. *Optics Express*, 12(8):1759–1768, 2004.

[5] A. S. Fokas, A. A. Himonas, and D. Mantzavinos. The nonlinear Schrödinger equation on the half-line. *Trans Am Math Soc*, 369(1):681–709, Mar. 2016.

[6] L. M. Frantz and J. S. Nodvik. Theory of Pulse Propagation in a Laser Amplifier. *J Appl Phys*, 34(8):2346–2349, 1963.

[7] J. Ghosh and B. Paden. A Pseudoinverse-Based Iterative Learning Control. *IEEE Trans Automat Contr*, 47(5):831–837, 2002.

[8] T. Glück, M. Blank, D. Büchl, and A. Kugi. Convex Constrained Iterative Learning Control Using Projection: Application to a Smart Power Switch. *IEEE Trans on Contr Syst Tech*, PP(99):1–8, 2017.

Post-print version of the article: A. Deutschmann, P. Malevich, A. Baltuska, and A. Kugi, “Modeling and iterative pulse-shape control of optical chirped pulse amplifiers”, *Automatica*, vol. 98, pp. 150–158, 2018, ISSN: 0005-1098. DOI: 10.1016/j.automatica.2018.09.002
The content of this post-print version is identical to the published paper but without the publisher's final layout or copy editing.

[9] D. Goswami. Optical pulse shaping approaches to coherent control. *Physics Reports*, 374(6):385–481, 2003.

[10] M. Grishin, V. Gulbinas, and A. Michailovas. Dynamics of high repetition rate regenerative amplifiers. *Optics Express*, 15(15):9434–9443, 2007.

[11] D. F. Hotz. Gain Narrowing in a Laser Amplifier. *Appl Optic*, 4(5):527–530, 1965.

[12] F. Krausz and M. Ivanov. Attosecond physics. *Rev of Mod Phys*, 81(1):163–234, 2009.

[13] P. Kroetz, A. Ruehl, K. Murari, H. Cankaya, F. X. Kärtner, I. Hartl, and R. J. D. Miller. Numerical study of spectral shaping in high energy Ho:YLF amplifiers. *Optics Express*, 24(9):9905, 2016.

[14] W. H. Lowdermilk and J. E. Murray. The multipass amplifier: Theory and numerical analysis. *J Appl Phys*, 51(5):2436–2444, 1980.

[15] P. Malevich, G. Andriukaitis, T. Flöry, A. J. Verhoef, A. Fernández, S. Ališauskas, A. Pugžlys, A. Baltuška, L. H. Tan, C. F. Chua, and P. B. Phua. High energy and average power femtosecond laser for driving mid-infrared optical parametric amplifiers. *Optic Lett*, 38(15):2746–2749, 2013.

[16] G. Métivier. The Mathematics of Nonlinear Optics. In *Handbook of Differential Equations: Evolutionary Equations*, volume 5, pages 169–313. Elsevier, 2009.

[17] T. Oksenhendler and N. Forget. Pulse-Shaping Techniques Theory and Experimental Implementations for Femtosecond Pulses. In M. Grishin, editor, *Advances in Solid State Lasers Development and Applications*. InTech, 2010.

[18] F. Omenetto, D. Reitze, B. Luce, M. Moores, and A. J. Taylor. Adaptive control methods for ultrafast pulse propagation in optical fibers. *IEEE J Sel Top Quant Electron*, 8(3):690–698, 2002.

[19] G. A. Reider. *Photonics: An Introduction*. Springer, 2 edition, 2016.

[20] B. Ren, P. Frihauf, M. Krstic, and R. J. Rafac. Laser Pulse Shaping via Iterative Learning Control and High-Dimensional Extremum Seeking. In *Proc ASME Dyn Syst Contr Conf*, pages 667–674, Arlington, USA, 2011.

[21] B. Ren, P. Frihauf, R. J. Rafac, and M. Krstic. Laser pulse shaping via extremum seeking. *Contr Eng Pract*, 20(7):674–683, 2012.

[22] B. E. A. Saleh and M. C. Teich. *Fundamentals of Photonics*. Wiley, 2 edition, 2007.

[23] A. E. Siegman. *Lasers*. University Science Books, Mill Valley, 1986.

[24] D. Strickland and G. Mourou. Compression of amplified chirped optical pulses. *Optic Comm*, 56(3):219–221, 1985.

[25] P. Tournois. Acousto-optic programmable dispersive filter for adaptive compensation of group delay time dispersion in laser systems. *Optic Comm*, 140(4–6):245–249, 1997.

[26] E. Treacy. Optical pulse compression with diffraction gratings. *IEEE J Quant Electron*, 5(9):454–458, 1969.

[27] E. V. Vanin, A. I. Korytin, A. M. Sergeev, D. Anderson, M. Lisak, and L. Vazquez. Dissipative optical solitons. *Phys Rev A*, 49(4):2806–2811, 1994.

[28] S. M. Webb, J. G. Ellison, S. R. Desbruslais, M. P. Fedoruk, and S. K. Turitsyn. Adaptive Pulse Shaping Through BER Feedback. *J Lightwave Tech*, 27(17):3765–3772, 2009.

[29] A. M. Weiner. Ultrafast optical pulse shaping: A tutorial review. *Optic Comm*, 284(15):3669–3692, 2011.

Post-print version of the article: A. Deutschmann, P. Malevich, A. Baltuska, and A. Kugi, "Modeling and iterative pulse-shape control of optical chirped pulse amplifiers", *Automatica*, vol. 98, pp. 150–158, 2018, ISSN: 0005-1098. DOI: 10.1016/j.automatica.2018.09.002
The content of this post-print version is identical to the published paper but without the publisher's final layout or copy editing.